Vibrational Properties of Disordered Mono- and Bilayers of Physisorbed Sulfur Hexafluoride on Au(111)†

A. W. Rosenbaum, M. A. Freedman, and S. J. Sibener*

The James Franck Institute and Department of Chemistry, The University of Chicago, 5640 South Ellis Ave., Chicago, Illinois 60637

Received: November 22, 2005; In Final Form: February 6, 2006

We have examined the low-energy single-phonon vibrations of disordered mono- and bilayers of sulfur hexafluoride physisorbed on Au(111) with inelastic helium atom scattering. At monolayer coverages, SF_6 exhibits a dispersionless Einstein mode at 3.6 ± 0.4 meV. We observed two distinct overtones of this vibration as both creation and annihilation events at 7.1 ± 0.7 meV and 10.9 ± 1.4 meV, respectively. The overtones are harmonic multiples of the fundamental Einstein oscillation. Bilayers of SF_6 exhibit a softer fundamental vibration with an excitation energy of 3.3 ± 0.3 meV. This softening, due to the weaker SF_6 binding, also results in reduced overtone energies of 6.6 ± 0.7 meV and 9.8 ± 0.6 meV. The disordered bilayer does not exhibit dispersion, indicating that the molecules are still behaving like Einstein oscillators and not beginning to act as bulk crystalline SF_6. The results have improved our understanding of the adsorbate−substrate and interadsorbate interactions which govern the properties of this model molecular physisorption system.

1. Introduction

Physisorbed noble gases have been studied extensively as model systems in surface science. Rare gases adsorbed on metal surfaces at cryogenic temperatures offer, in particular, key insights into adsorption kinetics, coverage dynamics, adatom diffusion, and crystal growth mechanisms.[1−7] The octahedral sulfur hexafluoride molecule exhibits many of the inert properties and rotationally averaged symmetry properties of rare gases, and thus represents an experimental adsorption system intermediate between rare gases and complex inorganic or organic thin films.[8−13]

Helium atom scattering (HAS) can probe the adsorbate−substrate and adsorbate−adsorbate interactions in a nonpertubative manner, giving insight into the state of mono- or multilayers. The deposition of rare gases (Ar, Xe, and Kr) on Ag(111) and Pt(111) has shown energetic and dispersive trends in phonon modes as a function of film thickness.[4,8,14,15] In these studies, it was found that a monolayer of a rare gas exhibits a low-energy dispersionless Einstein mode polarized perpendicular to the surface. The energy of this vibration softens, approaching the bulk rare gas frequency, with each additional layer because of the diminishing influence of interactions with the underlying substrate. The bilayer mode not only softens, but a dramatic change in the dispersion plot indicates that the intermolecular forces between the adatoms become increasingly important and alter the character of the vibrational mode observed. As the film thickness increases, the phonon modes continue to systematically approach the band structure of the surface Rayleigh wave of a bulk rare gas crystal.[13,16−18]

In this paper, we examine the vibrational characteristics of mono- and bilayer films of SF_6 adsorbed on Au(111). We do this to better understand the substrate−adsorbate and interadsorbate interactions of sulfur hexafluoride physisorbed on Au(111) and to examine the scaling properties of the operative interaction potentials which determine the condensed phase dynamics of this important molecular adsorption system. Numerous studies have examined the adsorption kinetics and structure of SF_6, ranging from bulk to physisorbed monolayers.[19−24] In bulk form, the translational motions of SF_6 freeze prior to rotational degrees of freedom, leading to an orientationally disordered bcc crystal from 96 to 223 K.[25−27] SF_6 in thin films or monolayers often does not retain the bulk structure, with structure imposed by the underlying surface.[22,23] The recent use of SF_6 as a dry etching gas has reopened studies into SF_6 adsorption. Interest has focused on cryogenic adsorption, negative ion resonance states,[28] and electron-stimulated desorption.[29−31] These studies look to elucidate interactions of SF_6 with both high-energy electrons and the substrate as critical components to controlling the dry etching processes.

Our studies of the librations of mono- and bilayers of SF_6/Au(111), in conjunction with the knowledge that comparable rare gas systems show bulk properties at fairly low coverages, could help refine the understanding of heat transfer in bulk molecular crystals. Purskii et al. have studied heat transfer in a variety of simple molecular crystals including bulk SF_6.[32−34] Investigating bulk SF_6 from 95 to 220 K, they find that the phonon−phonon coupling term is the dominant component of the thermal resistance of bulk SF_6. The phonon−rotation coupling term controls the line shape of the thermal resistance at higher temperatures likely due to an increase in orientational disorder, leading to a decrease in the correlation of neighboring molecular rotations. The thermal conductivity of bulk SF_6 approaches the diffusive heat transfer limit, as defined by Cahill et al. on the basis of a simple Einstein oscillator model, indicating that small wave vector vibrations play a key role in heat transfer.[35] These calculations rely strongly on the determination of the fundamental Einstein oscillations.

2. Experimental Section

Experiments were conducted in a high momentum- and energy-resolution helium atom scattering apparatus. Elastic and

† Part of the special issue "John C. Light Festschrift".

* To whom correspondence should be addressed. E-mail: s-sibener@uchicago.edu.

10.1021/jp0567772 CCC: $33.50
Published on Web 03/11/2006

inelastic scattering events are observed through diffraction and time-of-flight (TOF) measurements, respectively. This instrument has been described in detail elsewhere,[36,37] and its design will only be summarized here. It consists of a cryogenically cooled supersonic helium beam source, an ultrahigh-vacuum (UHV) scattering chamber equipped with appropriate surface characterization tools (such as LEED, AES, etc.), a precollision chopper (chopper-to-ionizer distance of 1.554 m), and a rotating, long flight path (sample-to-ionizer distance of 1.005 m) quadrupole mass spectrometer detector. The angular collimation yields a resolution of 0.22°, and the $\Delta v/v$ for most beam energies used is less than 1%. The Au(111) crystal used in these studies was prepared by repeated cycles of sputtering with 0.5 keV Ne^+ ions followed by annealing above 750 K, until contaminant levels were below our Auger detection limit and helium reflectivity was maximized. Surface crystallinity was confirmed by helium diffraction from the $(23 \times \sqrt{3})$ Au reconstruction[38,39] with average domain sizes greater than 400 Å, with this determination limited by the angular resolution of the apparatus.

Gaseous SF_6 (99.8% purity) was dosed by backfilling the scattering chamber, from a base pressure of 10^{-10} Torr to pressures of approximately 10^{-7} Torr to achieve varying exposures. Monolayer and submonolayer coverages were created by extended dosing near the overlayer desorption temperature (~105 K) followed by a quench to the scattering temperature, generally 85 K. SF_6 bilayers on Au(111) were created by dosing at 85 K for 120 s at 10^{-7} Torr. SF_6 coverage was quantified by comparing the Auger peak ratio for sulfur at 152 eV to Au at 239 eV and through helium atom reflectivity measurements during temperature programmed desorption (TPD). The temperature ramp rate for the TPD studies was 0.1 K per second.

3. Results

Figure 1a shows a typical TPD spectrum for monolayer coverage for a film deposited at 100 K. A similar deposition at 85 K, shown in Figure 1b, followed by a TPD exhibits both the mono- and bilayer desorption features. The bilayer film was prepared using a 120 s dose at 85 K. Auger electron spectroscopy (AES) was also used to quantify the coverage via the S/Au peak ratio. A prolonged exposure at a surface temperature of 105 K yields a S/Au Auger peak ratio of 3.75:1. An even longer dose at 85 K has a S/Au ratio of 7.5:1. The S/Au ratio of the extended low-temperature dose is twice the size of the warmer dose and cannot be increased by successive or longer doses at 85 K or higher temperatures. The combination of TPD and AES indicate the formation of mono- and bilayers of SF_6 and the inability to add a third layer of SF_6 because of the high initial sample temperature. After the deposition, time was allowed for the excess SF_6 to be evacuated from the chamber. Once the baseline pressure of the scattering chamber was reached, the TPD experiment was started. TPD spectra dosed at 85 K show two distinct features. The first feature occurs at a surface temperature of 105 K. This increase in signal is the result of bilayer SF_6 desorbing from the SF_6/Au(111) monolayer. The larger change in signal at approximately 110 K corresponds to the complete desorption of the monolayer. Figure 1a shows a similar experiment with an initial dosing temperature of 100 K in which only one desorption event is observed during the TPD, indicating monolayer or submonolayer coverage.

Helium atom diffraction along the $\langle 1\bar{1}0 \rangle$ azimuth was used to characterize the mono- and bilayers of SF_6/Au(111). Nonspecular features were absent from both systems, suggesting the absence of long-range surface order. Figure 2 shows a representative diffraction scan taken with a 22.8 meV beam at a specular scattering angle of 35.92°. Low-energy electron diffraction at a range of incident energies, 10−250 eV, also showed no indication of long-range adsorbate ordering beyond the underlying Au(111) spots observed at higher electron beam energies. Additional film preparation, such as annealing near the desorption temperature, did not produce Bragg diffraction rods during He scattering. We note X-ray and neutron diffraction

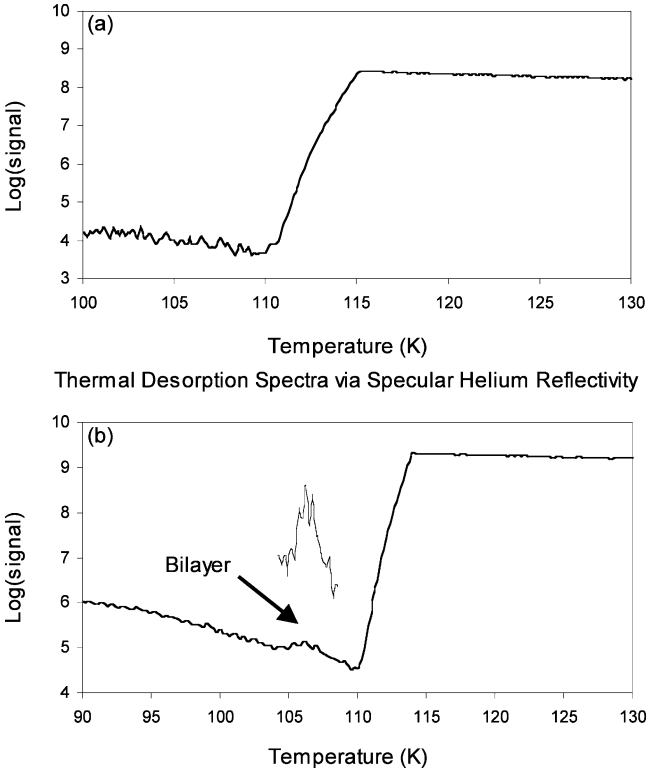

Figure 1. (a) A TPD spectrum taken using specular helium atom reflectivity showing desorption of a monolayer. SF_6 was dosed at a background pressure of 10^{-7} Torr for 120 s at a sample temperature of 100 K. Upon completion of the dose, the temperature was ramped through the desorption regime at a rate of 0.1 K per second. The rapid increase in signal at 110 K indicates desorption of the monolayer. (b) An example of a TPD spectrum taken using helium atom reflectivity to monitor the surface coverage of SF_6. SF_6 was introduced at a sample temperature of 85 K for 120 s at a pressure of 10^{-7} Torr. After the residual gas was pumped out, the sample temperature was ramped at a rate of 0.1 K per second through two distinct desorption events. The arrow indicates the bilayer desorption at 105 K. The inset enlarges the bilayer desorption event. Monolayer desorption follows at 110 K when the signal rapidly recovers to the predose level.

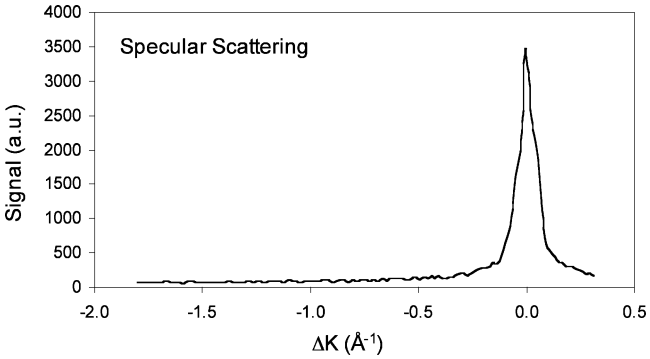

Figure 2. A representative He diffraction scan along the $\langle 1\bar{1}0 \rangle$ azimuth from a monolayer of SF_6 physisorbed on Au(111). The specular scattering angle was 35.92° with a beam energy of 22.8 meV. In this scan, no subspecular peaks are observed. No superspecular peaks are observed in the complimentary He diffraction scans.

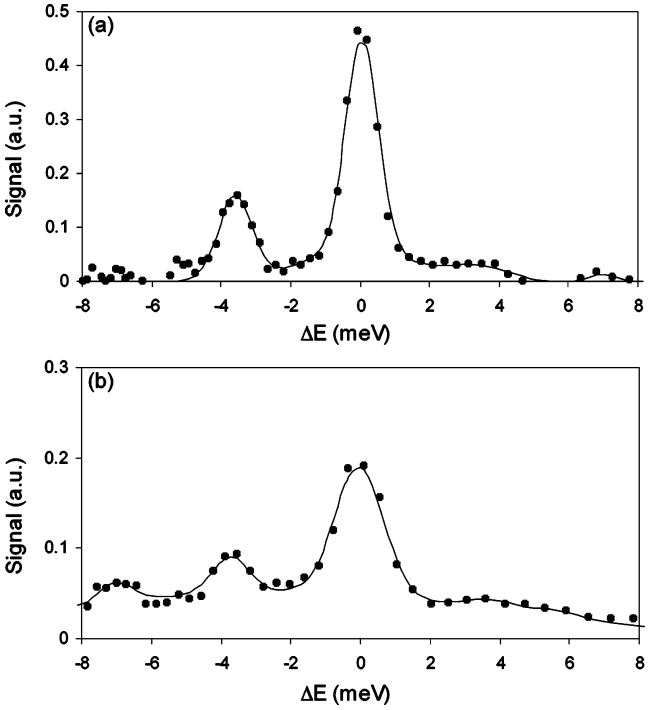

Figure 3. (a) A representative TOF spectrum with a 19.0 meV He beam shows both creation and annihilation events at 3.6 meV from a monolayer of SF_6 at 80 K. The data are shown by the filled circles. The line through the data is a least-squares fit using five Gaussian curves, for the elastic, single, and multiphonon events, and a linear background. The incident and final scattering angles were 35.92° and 33.92°, respectively. (b) A representative TOF spectrum taken with a 25.5 meV beam showing both the fundamental excitation, 3.6 meV, and its harmonic overtone, seen at 7.1 meV from a monolayer of SF_6 at 85 K. The data are shown by the filled circles. The line through the data is a least-squares fit using five Gaussian curves, for the elastic, single, and multiphonon events, and a linear background. The incident and final scattering angles are 35.92° and 37.92°, respectively.

studies found that bulk SF_6 forms a bcc crystal above 95 K and a more complicated monoclinic structure at lower temperatures.[25,26] X-ray diffraction found monolayer SF_6 adsorbed on graphite also undergoes a transformation from a commensurate (2×2) structure below 95 K to an incommensurate hexagonal structure at higher surface temperatures.[22]

Figure 3a shows a characteristic TOF spectrum taken with a 19.0 meV He beam scattering from a monolayer of SF_6 at a sample temperature of 80 K. The TOF shows both creation and annihilation events associated with the 3.3 meV phonon. For a complete sampling of the phonon modes, it is necessary to vary both beam energy and scattering angles. Higher beam energies will increase the propensity to excite overtones but also diminish the signal-to-noise ratio due to a rise in multiphonon scattering. After sampling from a range of beam energies (15.5−33.4 meV), Figure 3b exhibits data collected with the beam energy considered optimal and most frequently used, 25.5 meV. Each elastic, inelastic, and multiphonon feature in the inelastic spectra was fit with a Gaussian line shape. The width of the fitted peaks was allowed to vary.

The excitation energy of the fundamental vibration of the SF_6/Au(111) monolayer remains constant regardless of the scattering condition. Figure 4 shows a dispersion plot (ΔK vs ΔE) using a variety of beam energies while varying the range of incident angles, from 25.92° to 35.92°, and final angles, from 26.92° to 38.92°. Both fundamental annihilation and creation events are seen at sub- and superspecular scattering angles. The data obtained for the dispersion plots span 0.6 $Å^{-1}$, which is

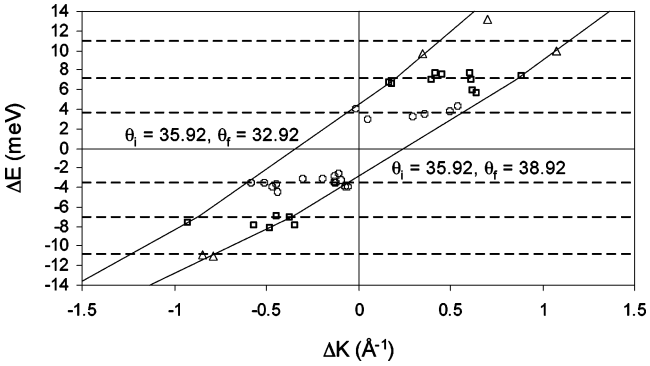

Figure 4. The dispersion plot, ΔK vs ΔE, for the fundamental phonon and harmonic overtones for monolayer SF_6/Au(111). Dashed horizontal lines indicate the average creation and annihilation energies. The solid lines running diagonally are two representative scan curves. The data come from a variety of beam energies ranging from 19.0 to 33.5 meV and incident angles from 35.92° to 25.92° with exit angles from 38.92° to 24.92°. Circles, squares, and triangles represent the fundamental, first overtone, and second overtone events, respectively.

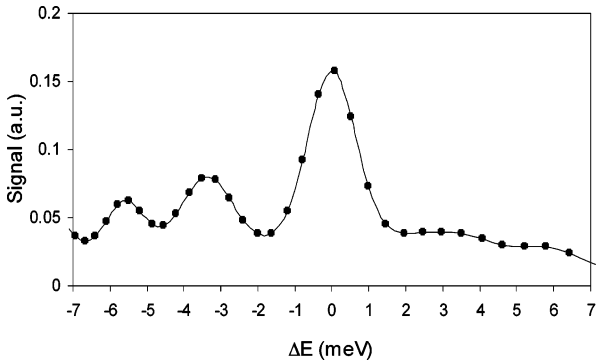

Figure 5. A representative TOF spectrum taken from bilayer SF_6 at a surface temperature of 85 K with a 25.5 meV beam. The fundamental and harmonic excitations of the bilayer occur at 3.3 ± 0.3 meV and 6.6 ± 0.7 meV, respectively. The data are shown by the filled circles. The line through the data is a least-squares fit using six Gaussian curves, for the elastic, single, and multiphonon events, and a linear background. The incident and final scattering angles are 35.92° and 37.92°, respectively.

approximately half the distance to the zone edges of Au(111) of 1.452 and 1.257 $Å^{-1}$ and greater than half the distance for bulk crystalline SF_6 below 94 K.[25]

At higher beam energies, we excite more phonons, as shown in Figure 3b. The higher-energy phonon, seen at 7.1 meV in both creation and annihilation events, is the first harmonic overtone. This overtone is found in a large number of spectra, while the second overtone, seen at 10.9 meV, is often masked by multiphonon scattering. The dispersion plot for the overtones is shown in Figure 4.

Inelastic scattering from a bilayer of SF_6/Au(111) taken with a 25.5 meV beam is shown in Figure 5. The fundamental annihilation and creation events are shifted to lower energies, which in turn reduce the excitation energy of the overtones. The phonon remains dispersionless with harmonic overtones seen at 6.6 and 9.8 meV, as shown in Figure 6. The data obtained for this dispersion plot again span approximately 0.6 $Å^{-1}$. Because of the low signal and the multiphonon background, the uncertainties in the peak positions of the overtone modes are greater than for the fundamental modes for both the mono- and bilayer systems. These uncertainties fluctuate randomly as seen in the dispersion plots, which indicates that no dispersion is occurring.

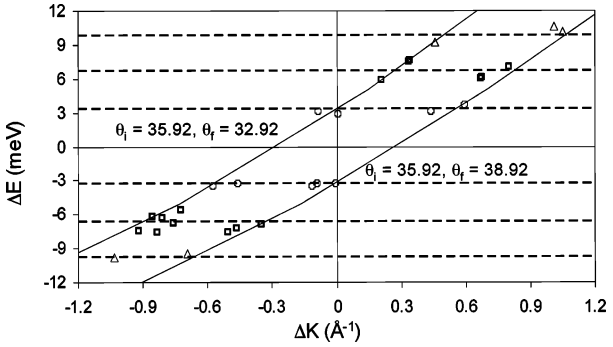

Figure 6. The dispersion plot, ΔK vs ΔE, for the fundamental and harmonic overtones for bilayer SF_6/Au(111). Dashed horizontal lines indicate the average creation and annihilation energies. The solid lines running diagonally are two representative scan curves. The data shown come from a variety of beam energies ranging from 19.0 to 25.5 meV, an incident angle of 35.92°, and final angles from 32.92° to 38.92°. Circles, squares, and triangles represent the fundamental, first overtone, and second overtone events, respectively.

4. Discussion

From the inelastic scattering, we extracted the Debye−Waller factor, $2W$, over the temperature range used in this study of SF_6/Au(111). Since both the mono- and bilayers of SF_6/Au(111) exhibit Einstein phonons, we can use the following formulation to get the mean square displacements[40]

$$\langle u_z^2 \rangle = \left(\frac{\hbar}{2M\omega}\right) \coth\left(\frac{\hbar\omega}{2k_bT}\right) \tag{1}$$

where M is the mass of the vibrating surface, T is the surface temperature, $\hbar$ is Planck's constant, k_b is Boltzmann's constant, ω is the fundamental frequency of the Einstein vibration, and $\langle u_z^2 \rangle$ is the surface normal mean square displacement.

Using the fundamental vibrational frequencies for the mono- and bilayers, we get mean square displacements at 85 K of 1.7×10^{-2} and 2.0×10^{-2} Å^2, respectively. As expected, the bilayer has a wider range of motion, 18% greater than the monolayer, due to the diminished interaction with the substrate. These displacements can be converted into Debye−Waller factors for a particular surface temperature by accounting for the perpendicular momentum transfer while scattering at specular to eliminate the component from the parallel momentum transfer

$$2W = \Delta k_z^2 \langle u_z^2 \rangle \tag{2}$$

where W is the Debye−Waller factor, Δk_z is the perpendicular momentum transfer, and $\langle u_z^2 \rangle$ is the perpendicular mean square displacement. The slope of the lines prior to desorption in Figure 1a,b can also be used to determine the Debye−Waller factor and thus the surface motion of the mono- and bilayers.

$$I = I_0 \, e^{-2W} \tag{3}$$

Using these slopes and accounting for the scattering conditions, the bilayer has a 16% greater range of motion than the monolayer. This result agrees with the calculation based on eq 1.

The mono- and bilayer SF_6 mean square displacements can be compared with displacements calculated from fundamental vibrational energies at 85 K for Ar, Kr, and Xe monolayers on Ag(111) of 5.8×10^{-2}, 4.4×10^{-2}, and 3.0×10^{-2} Å^2 respectively.[2] While the comparison involves two different substrates, the interaction terms of rare gases with Au and Ag have been well-documented and are within 10%.[41,42] SF_6 continues the trend of decreasing mean square displacement with increased mass and polarizability. Prior studies indicate that physical adsorption potentials of rare gases adsorbed on metal surfaces have the same shape and are scalable.[43] A theoretical study using the fundamental vibrational modes, potential well depths, and van der Waals C_3 coefficients could be used to determine if the adsorption potential for SF_6/Au(111) has the same shape as physisorbed rare gases on metals.[43]

While the rare gas and SF_6 monolayers behave in a similar fashion, the bilayers show significantly different behavior. The rare gas bilayers show significant increases, 30−50%, in mean square displacement in comparison to their respective monolayers, while the motion of the SF_6 bilayer increases only by 16−19%. This difference in displacement can be explained by considering the significantly larger van der Waals C_6 coefficient and polarizability of SF_6 when compared to rare gases, as discussed below.[5,44−46] Luo et al. found that interlayer force constants taken with respect to the substrate−adsorbate interaction define the trend in phonon frequency as a function of film thickness.[15] The smaller change in SF_6/Au(111) vibrational energy, and thus displacement, from mono- to bilayer is simply a function of the increased interaction term between layers as compared to that of rare gases.

To understand the reduced mobility of the bilayer of SF_6 compared to noble gases, the reduced potential curves can be compared. The reduced Morse potential, which can be used around the equilibrium internuclear distance r_m, is given by

$$V(x) = \exp[-2\beta(x-1)] - 2\exp[-\beta(x-1)] \tag{4}$$

where β is the ratio of the Morse potential parameter and r_m, and x is the ratio of the internuclear separation and r_m. Barker et al. showed that the rare gas dimer potentials have similar reduced parameters, indicating that the reduced potentials fall on a universal curve.[47] While SF_6 dimers have a smaller well depth ϵ and larger internuclear separation r_m than Xe_2, the curvature of the potential well is such that the reduced potential of an SF_6 dimer coincides with the rare gases (He_2, Ne_2, Ar_2, Kr_2, Xe_2).[48,49] At larger internuclear separations where the potential is dominated by the van der Waals constant C_6, a deviation from the universal curve appropriate for the rare gas dimers arises. While the van der Waals constant is significantly greater than for the rare gases,[46] the reduced constant $C_6^* = C_6/\epsilon r_m^6$ is much smaller because of the larger internuclear separation. It would therefore not be expected that SF_6 should follow the trends observed for rare gases. The increased C_6 of SF_6 should lead to larger long-range interactions, suppressing motion on the surface.

The band structure of the SF_6 bilayer also departs from ordered rare gas overlayers. The phonon mode of the bilayer does soften energetically, but there is no indication of the dispersion seen in similar rare gas systems as the coverage increases.[4] The dispersionless mode indicates that the properties of the bilayer are still far from those of bulk crystalline SF_6. The lack of collective motions is due to the disordered underlying layer and keeps the bilayer of SF_6/Au(111) in the independent oscillator regime. In particular, the underlying disorder removes collective interlayer interactions imperative to dispersion.[50] Future directions might involve increasing the SF_6 coverage systematically with a colder substrate and longer exposure times to track the onset of bulk crystalline surface properties. Subsequent studies might also explore the effects of the molecular environment including the underlying phonon density of states of the substrate via examination of wavevector-resolved line shapes and scattering probabilities.

In summary, we have identified a dispersionless Einstein mode in disordered mono- and bilayers of SF_6 physisorbed on Au(111). The SF_6 adsorbs in a disordered state, showing no Bragg diffraction rods indicative of crystalline order. The fundamental phonon mode and the harmonic overtones for the monolayer are observed at 3.6 ± 0.4 meV, 7.1 ± 0.7 meV, and 10.9 ± 1.4 meV, respectively. The fundamental mode then softens to 3.3 ± 0.3 meV for the second layer as the influence of the substrate is diminished. The overtones for the bilayer, seen at 6.6 ± 0.7 meV and 9.8 ± 0.6 meV, remain harmonic and dispersionless. While the mode softens for bilayer coverage, it remains dispersionless because of its disorder, leaving the system in an independent oscillator regime. These results have improved our understanding of the adsorbate−substrate and interadsorbate interactions which govern the properties of this model molecular physisorption system.

Acknowledgment. We thank Kevin Gibson for sharing his expertise regarding helium scattering from physisorbed species. This work was primarily supported by the Chemical Sciences, Geosciences and Biosciences Division, Office of Basic Energy Sciences, Office of Science, U.S. Department of Energy, grant DE-FG02-00ER15089. We also acknowledge supplemental infrastructure support from the NSF-Materials Research Science and Engineering Center at the University of Chicago, NSF-DMR-0213745. M.A.F. gratefully acknowledges support through a National Science Foundation Graduate Research Fellowship.

References and Notes

(1) Cohen, P. I.; Unguris, J.; Webb, M. B. *Surf. Sci.* **1976**, *58*, 429.
(2) Gibson, K. D.; Sibener, S. J. *J. Chem. Phys.* **1988**, *88*, 7862.
(3) Gibson, K. D.; Cerjan, C.; Light, J. C.; Sibener, S. J. *J. Chem. Phys.* **1988**, *88*, 7911.
(4) Gibson, K. D.; Sibener, S. J. *J. Chem. Phys.* **1988**, *88*, 7893.
(5) Bruch, L. W.; Cole, M. W.; Zaremba, E. *Physical Adsorption: Forces and Phenomena*; Oxford University Press, Inc.: New York, 1997; Vol. 33.
(6) Kern, K.; Zeppenfeld, P.; David, R.; Comsa, G. *Phys. Rev. B* **1987**, *35*, 886.
(7) Siber, A.; Gumhalter, B.; Braun, J.; Graham, A. P.; Bertino, M. F.; Toennies, J. P.; Fuhrmann, D.; Woll, C. *Phys. Rev. B* **1999**, *59*, 5898.
(8) Kern, K.; David, R.; Palmer, R. E.; Comsa, G. *Phys. Rev. Lett.* **1986**, *56*, 2823.
(9) Rosenbaum, A. W.; Freedman, M. A.; Darling, S. B.; Popova, I.; Sibener, S. J. *J. Chem. Phys.* **2004**, *120*, 3880.
(10) Darling, S. B.; Rosenbaum, A. W.; Sibener, S. J. *Surf. Sci.* **2001**, *478*, L313.
(11) Darling, S. B.; Rosenbaum, A. W.; Wang, Y.; Sibener, S. J. *Langmuir* **2002**, *18*, 7462.
(12) *Self-Assembled Monolayers of Thiols*; Ulman, A., Ed.; Academic Press: San Diego, CA, 1998; Vol. 24.
(13) Gibson, K. D.; Sibener, S. J. *Phys. Rev. Lett.* **1985**, *55*, 1514.
(14) Cardini, G. G.; O'Shea, S. F.; Marchese, M.; Klein, M. L. *Phys. Rev. B* **1985**, *32*, 4261.
(15) Luo, N. S.; Ruggerone, P.; Toennies, J. P. *Phys. Rev. B* **1996**, *54*, 5051.
(16) Siber, A.; Gumhalter, B.; Graham, A. P.; Toennies, J. P. *Phys. Rev. B* **2001**, *63*, 115411.
(17) Gibson, K. D.; Sibener, S. J.; Hall, B. M.; Mills, D. L.; Black, J. E. *J. Chem. Phys.* **1985**, *83*, 4256.
(18) Gibson, K. D.; Sibener, S. J. *Faraday Discuss. Chem. Soc.* **1985**, *80*, 203.
(19) Klekamp, A.; Umbach, E. *Chem. Phys. Lett.* **1990**, *171*, 233.
(20) Taylor, J. C.; Waugh, A. B. *J. Solid State Chem.* **1976**, *18*, 241.
(21) Klekamp, A.; Umbach, E. *Surf. Sci.* **1991**, *249*, 75.
(22) Marti, C.; Ceva, T.; Croset, B.; Beauvais, C. D.; Thomy, A. *J. Phys. (Paris)* **1986**, *47*, 1517.
(23) Bouchdoug, M.; Ceva, T.; Marti, C.; Menaucourt, J.; Thomy, A. *Surf. Sci.* **1985**, *162*, 426.
(24) Fisher, G. B.; Erikson, N. E.; Madey, T. E.; Yates, J. T. *Surf. Sci.* **1977**, *65*, 210.
(25) Isakina, A. P.; Prokhvatilov, A. I. *Low Temp. Phys.* **1993**, *19*, 142.
(26) Dolling, G.; Powell, B. M.; Sears, V. F. *Mol. Phys.* **1979**, *37*, 1859.
(27) Michel, J.; Drifford, M.; Rigny, P. *J. Chim. Phys.* **1970**, *67*, 31.
(28) Siller, L.; Vanter, N.; Palmer, R. E. *Surf. Sci.* **2000**, *465*, 76.
(29) Faradzhev, N. S.; Kusmierek, D. O.; Yakshinskiy, B. V.; Solovev, S. M.; Madey, T. E. *Surf. Sci.* **2003**, *528*, 20.
(30) Faradzhev, N. S.; Kusmierek, D. O.; Yakshinskiy, B. V.; Madey, T. E. *Low Temp. Phys.* **2003**, *29*, 215.
(31) Souda, R.; Gunster, J. *Phys. Rev. A* **2003**, *67*, 1.
(32) Purskii, O. I.; Zholonko, N. N.; Konstantinov, V. A. *Low Temp. Phys.* **2000**, *26*, 278.
(33) Purskii, O. I.; Zholonko, N. N.; Konstantinov, V. A. *Low Temp. Phys.* **2003**, *29*, 771.
(34) Purskii, O. I.; Zholonko, N. N. *Phys. Solid State* **2004**, *46*, 2015.
(35) Cahill, D. G.; Watson, S. K.; Pohl, R. O. *Phys. Rev. B* **1992**, *46*, 6131.
(36) Niu, L.; Koleske, D. D.; Gaspar, D. J.; Sibener, S. J. *J. Chem. Phys.* **1995**, *102*, 9077.
(37) Gans, B.; King, S. F.; Knipp, P. A.; Koleske, D. D.; Sibener, S. J. *Surf. Sci.* **1992**, *264*, 81.
(38) Harten, U.; Lahee, A. M.; Toennies, J. P.; Wöll, C. *Phys. Rev. Lett.* **1985**, *54*, 2619.
(39) Barth, J. V.; Brune, H.; Ertl, G.; Behm, R. J. *Phys. Rev. B* **1990**, *42*, 9307.
(40) Ellis, T. H.; Scoles, G.; Valbusa, U. *Chem. Phys. Lett.* **1983**, *94*, 247.
(41) Zaremba, E. *Surf. Sci.* **1985**, *151*, 91.
(42) Vidali, G.; Ihm, G.; Kim, H.-Y.; Cole, M. W. *Surf. Sci. Rep.* **1991**, *12*, 133.
(43) Vidali, G.; Cole, M. W.; Klein, J. R. *Phys. Rev. B* **1983**, *28*, 3064.
(44) Standard, J. M.; Certain, P. R. *J. Chem. Phys.* **1985**, *83*, 3002.
(45) Pack, R. T. *J. Phys. Chem.* **1982**, *86*, 2794.
(46) Kumar, A.; Fairley, G. R. G.; Meath, W. J. *J. Chem. Phys.* **1985**, *83*, 70.
(47) Barker, J. A.; W., R. O.; Lee, J. K.; Schafer, T. P.; Lee, Y. T. *J. Chem. Phys.* **1974**, *61*, 3081.
(48) MacCormack, K. E.; S., W. G. *J. Chem. Phys.* **1951**, *19*, 849.
(49) Farrar, J. M.; S., T. P.; Lee, Y. T. *AIP Conf. Proc.* **1973**, *11*, 279.
(50) Woll, C. *Appl. Phys. A* **1991**, *53*, 377.